MIT Libraries | DSpace@MIT

MIT Open Access Articles

Study on Stiffness and Conditioning Effects of CMP Pad Based on Physical Die-Level CMP Model

The MIT Faculty has made this article openly available. ***Please share*** how this access benefits you. Your story matters.

Citation: Fan, Wei et al. “Study on Stiffness and Conditioning Effects of CMP Pad Based on Physical Die-Level CMP Model.” Journal of The Electrochemical Society 157.5 (2010): H526. ©2010 The Electrochemical Society

Published Version: http://dx.doi.org/10.1149/1.3369963

Publisher: Electrochemical Society

Permanent Link: http://hdl.handle.net/1721.1/71165

Version: Final published version: final published article, as it appeared in a journal, conference proceedings, or other formally published context

Terms of use: Article is made available in accordance with the publisher's policy and may be subject to US copyright law. Please refer to the publisher's site for terms of use.

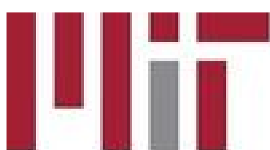

Massachusetts Institute of Technology

Journal of The Electrochemical Society, **157** (5) H526-H533 (2010)
0013-4651/2010/157(5)/H526/8/$28.00 © The Electrochemical Society

Study on Stiffness and Conditioning Effects of CMP Pad Based on Physical Die-Level CMP Model

Wei Fan,[a,z] Duane Boning,[a,*] Leslie Charns,[b] Hiroyuki Miyauchi,[c] Hiroyuki Tano,[c] and Shoei Tsuji[c]

[a]*Department of Electrical Engineering and Computer Science, Massachusetts Institute of Technology, Cambridge, Massachusetts 02139, USA*
[b]*JSR Micro Incorporated, Sunnyvale, California 94089, USA*
[c]*JSR Corporation, Yokkaichi Research Center, Yokkaichi 510-8552, Japan*

Chemical mechanical planarization (CMP) pad stiffness and conditioning effects were evaluated based on a physical die-level CMP model, with pad effective modulus and asperity height as parameters. In one study, patterned dielectric wafers were polished using polymeric pads of different stiffnesses. In a second study, wafers were polished by standard pads using different conditioning disks. Polishing experimental data (dielectric thickness and step height) were fitted by the physical model, enabling the extraction of the pad effective modulus and asperity height model parameters. A higher pad stiffness gives better within-die uniformity, and the conditioning disk with blocky diamonds achieves up-area only polishing for longer times. Polishing simulations using the physical model reflect a clear pattern density dependence.
© 2010 The Electrochemical Society. [DOI: 10.1149/1.3369963] All rights reserved.

Manuscript submitted December 3, 2009; revised manuscript received March 1, 2010. Published April 1, 2010.

Chemical mechanical planarization (CMP) is a key process in modern integrated circuit (IC) fabrication.[1] It is widely used in the front end for device isolation (such as shallow trench isolation) and building advanced device structures and in the back end for dielectric planarization and metal damascene formation.[2] CMP combines chemical and mechanical interactions to polish metal and dielectric surfaces using a slurry composed of chemicals and submicrometer particles. The slurry is fed onto a polishing pad made of a porous polymer. By moving the pad across the wafer in a circular, elliptical, or linear motion, the wafer surface is polished.[3]

To understand the CMP process, various models have been proposed.[4] CMP models can be roughly categorized into three classes: particle-level models, die-level models, and wafer-level models. Particle-level models seek to understand the material polishing mechanism of CMP, such as chemical pH and abrasive size effects. Die-level models study the polishing of an entire die or IC chip. They focus on the planarization capability of CMP, i.e., modeling the reduction or evolution in the height of topographical structures on the wafer surface. Wafer-level models are used when the CMP system effects are important, such as nonuniform distribution of pressure, slurry concentration, and temperature across the wafer.

In our previous work, a physical die-level CMP model was developed based on contact mechanics to understand and optimize the dielectric planarization process.[5] The model can be used to simulate the wafer surface evolution in the CMP process, as well as to study how planarization is affected by pad properties and process conditions.

In this paper, specific CMP pad properties are related to our CMP model parameters, enabling us to clarify how pad bulk and surface properties affect within-die planarization. The effects of pad stiffness and conditioning disk diamond shape are investigated so as to intentionally modify pad bulk and surface properties, and fits of the model to experimental data from the polishing of patterned wafers are used to relate planarization model parameters to pad properties. Die-level uniformity is predicted by simulation under different CMP end-point strategies.

In the following section, we first introduce our physical die-level CMP model including model framework and parameters. Then, the Experimental section explains the polishing experiments and measurements. Lastly, we separately discuss pad stiffness effect, conditioning disk effect, and CMP die-level uniformity in the Results and Discussion section.

* Electrochemical Society Active Member.
[z] E-mail: fanwei@mit.edu

Physical Die-Level CMP Model

Our physical die-level CMP model describes the dependence of pressures on the local pattern density and surface step height of a single die. It assumes that the elastomeric polishing pad can be decomposed into bulk and asperity regions, as shown in Fig. 1. The bulk material can be treated as an elastic body, deforming in response to long-range wafer height differences. The surface asperities come in contact with the wafer surface, and the compression of the asperities depends on both the wafer surface profile and the pad bulk bending. Figure 2 illustrates the model framework and the coordinate system. The wafer is assumed to press into the polishing pad in the positive Z direction. For convenience, the surface normal of the wafer is taken as the positive Z direction, corresponding to the conventional "wafer face up" mathematical representation. Here, $w(x,y)$ is used to describe the z-coordinate of the nominal separation point between the bulk and the asperities of the pad, and $z(x,y)$ is used to describe the wafer surface. The distance between the wafer surface and the nominal bulk pad position is $w(x,y) - z(x,y)$.

Modeling of bulk.— The bulk is elastic and can be modeled using a contact wear model.[6,7] The relationship between the bulk surface displacement $w(x,y)$ and pressure $P(x,y)$ satisfies the following convolution

$$w(x,y) - w_0 = F(x,y) \otimes P(x,y) \quad [1]$$

where $F(x,y)$ is the deformation response to a point pressure. This deformation is proportional to $1/E$, where E is the effective modulus of the pad. Here, w_0 is the relative reference plane of the bulk surface when there is no pressure applied. For mathematical convenience, w_0 is set to zero. The boundary condition applied to Eq. 1 is

$$\frac{1}{S}\int_S P(x,y)dxdy = P_0 \quad [2]$$

where P_0 is the reference pressure applied to the bulk and S is the contact area. Equation 2 indicates that the bulk response force is equal to the force applied from the outside.

Modeling of asperities.— The asperities are assumed to have a negligible width and an exponential height distribution.[8] Equation 3 defines the distribution with a characteristic asperity height λ

$$l(\xi) = \frac{1}{\lambda}e^{-\xi/\lambda} \quad [3]$$

where ξ is the asperity height. At location (x,y), the distance between the wafer surface $z(x,y)$ and the nominal plane $w(x,y)$ is

Downloaded 14 Jun 2012 to 18.51.3.76. Redistribution subject to ECS license or copyright; see http://www.ecsdl.org/terms_use.jsp

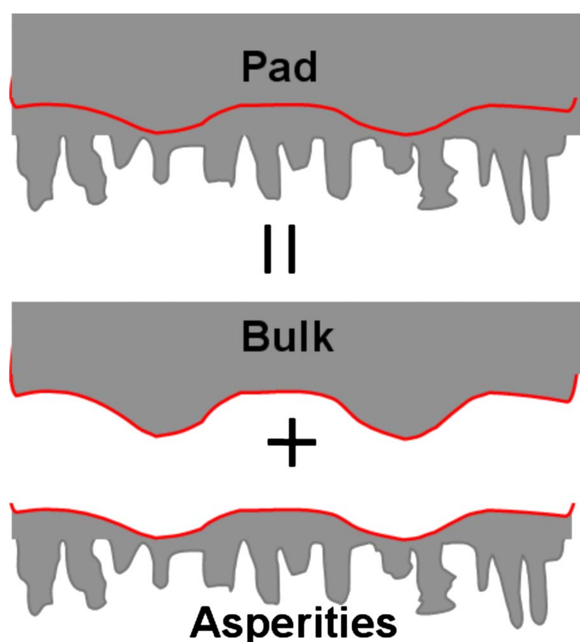

Figure 1. (Color online) Pad structure assumption in physical die-level CMP model. The whole pad is comprised of bulk and asperities.

$w(x,y) - z(x,y)$, so asperities of height ξ larger than $w(x,y) - z(x,y)$ contact the wafer surface, and the amount of compression of these asperities is $\xi - [w(x,y) - z(x,y)]$. All the asperities are assumed to obey Hooke's law; i.e., the exerting force is proportional to the compressed amount. The expected value of $P(x,y)$ can be estimated by averaging across all the asperities as follows

$$P(x,y) = \int_{w(x,y)-z(x,y)}^{\infty} k\{\xi - [w(x,y) - z(x,y)]\}l(\xi)d\xi = k\Psi[w(x,y) - z(x,y)] \quad [4]$$

where k is a spring constant and $\Psi(z)$ is a derived asperity height distribution function, defined as $\Psi(z) = \int_z^{\infty}(\xi - z)l(\xi)d\xi$. $\Psi(z)$ can be calculated once the probability distribution of asperity height is known, and it is a strictly decreasing function and approaches zero at infinity. Because we assume the asperity height distribution as given in Eq. 3, $\Psi(z)$ is given by

$$\Psi(z) = \lambda e^{-z/\lambda} \quad [5]$$

When a feature of step height $h(x,y)$ is pressed against the pad, as shown in Fig. 2, Eq. 4 implies that the up-area pressure is

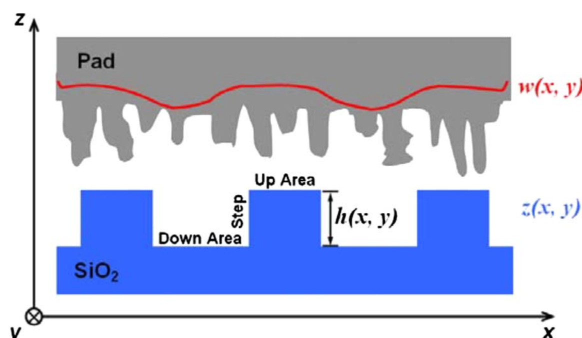

Figure 2. (Color online) Framework of physical die-level CMP model.

$$P_u(x,y) = k\Psi[w(x,y) - z_u(x,y)] \quad [6]$$

and the down-area pressure is

$$P_d(x,y) = k\Psi[w(x,y) - z_u(x,y) + h(x,y)] \quad [7]$$

The total local pressure is the sum of the two pressures weighted by pattern density $\rho(x,y)$, which is the area fraction of the up area. So, we have

$$P(x,y) = \rho(x,y)P_u(x,y) + [1 - \rho(x,y)]P_d(x,y) = \rho(x,y)k\Psi[w(x,y) - z_u(x,y)] + [1 - \rho(x,y)]k\Psi[w(x,y) - z_u(x,y) + h(x,y)] \quad [8]$$

Combining Eq. 5-8, we relate the pressures to the step height and characteristic asperity height as follows

$$P(x,y) = k\{\rho(x,y) + [1 - \rho(x,y)]e^{-h(x,y)/\lambda}\}\lambda e^{-w(x,y)-z_u(x,y)/\lambda}$$

$$P_d(x,y) = \frac{1}{1 + \rho(x,y)(e^{h(x,y)/\lambda} - 1)}P(x,y)$$

$$P_u(x,y) = \frac{e^{h(x,y)/\lambda}}{1 + \rho(x,y)(e^{h(x,y)/\lambda} - 1)}P(x,y) \quad [9]$$

Modeling of CMP process.— The physical CMP model can be obtained by combining the effects of the two parts above together: the elastic pad bulk, which is described by Eq. 1, and the asperities with exponential height distribution, which is described by Eq. 9. The pressure and deflection interactions between wafer surface topography and CMP pad are therefore described by

$$P(x,y) = k\{\rho(x,y) + [1 - \rho(x,y)]e^{-h(x,y)/\lambda}\}\lambda e^{-w(x,y)-z_u(x,y)/\lambda}$$

$$w(x,y) = F(x,y) \otimes P(x,y) + w_0 \quad [10]$$

To run the model, pattern density $\rho(x,y)$ needs to be extracted from the die layout. With initial values of step height and up-area coordinate, the two unknowns $P(x,y)$ and $w(x,y)$ can be calculated by solving Eq. 10 iteratively. Once $P(x,y)$ is solved, $P_u(x,y)$ and $P_d(x,y)$ can be obtained by Eq. 9. Then, the model employs Preston's equation[9] with local pressure $P(x,y)$ to calculate the instantaneous material removal rates of the up and down areas as follows

$$\frac{dz(x,y)}{dt} = -K_p P(x,y)v \quad [11]$$

where K_p is the Preston coefficient and v is the linear velocity of the pad relative to the wafer. So, $z_u(x,y)$ and $h(x,y)$ are dynamically updated during the simulation of CMP.

Model parameters.— There are three key parameters in the physical die-level CMP model: blanket removal rate K_0, effective modulus E, and characteristic asperity height λ. The blanket removal rate is affected by many CMP tools, consumable, and process parameters, such as the CMP system reference pressure. The effective modulus is related to the properties of the pad bulk and is hypothesized to most strongly impact within die uniformity and layout pattern density effects, resulting from long-range pad bending due to differential removal rates in different die pattern density regions. The characteristic asperity height reflects the distribution of pad asperity heights and is hypothesized to most strongly impact the feature scale step height reduction. The pad property related parameters, E and λ, are independent of each other; in the model we assume the CMP pad can be divided into two parts, pad bulk and asperities. E is only affected by the pad bulk stiffness, while λ is only affected by the pad surface asperity height distribution. Thus, extracting these two independent parameters from experimental data enables separate investigations of the pad bulk and surface properties.

Downloaded 14 Jun 2012 to 18.51.3.76. Redistribution subject to ECS license or copyright; see http://www.ecsdl.org/terms_use.jsp

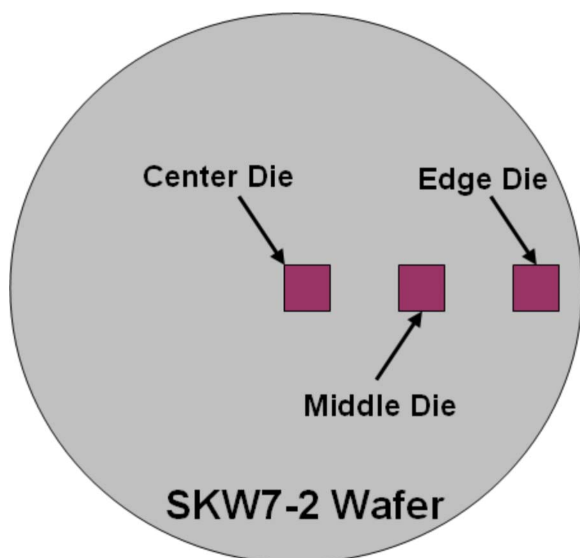

Figure 3. (Color online) Optical measured die positions on a SKW7-2 dielectric wafer.

Experimental

To evaluate the effect of pad stiffness, three water soluble particle (WSP) pads[10-12] (produced by JSR Corporation) were engineered to have different stiffnesses (low, standard, and high) and were used in patterned wafer polishing. In the conditioning disk effect study, three conditioning disks with different diamond shapes (sharp, standard, and blocky) were applied on JSR standard pads. These diamond shapes were expected to "cut" into the pad surface differently, generating different pad asperity surface structures.

SKW7-2 oxide wafers patterned with a Massachusetts Institute of Technology CMP test layout[13] were polished using JSR WSP pads. We varied the pad stiffness and the conditioning disk diamond shape separately, while the CMP machine recipe was kept all the same. Each test wafer was polished under a reference pressure of 5 psi for different times accumulative to more than 2 min: 0, 20, 40, 70, 90, 110, and 130 s.

Optical measurements of film thickness and step height were performed after polishing. On each wafer, we selected a center die, a middle die, and an edge die to test, as shown in Fig. 3. Figure 4 shows the pattern type and local pattern density within each die of the SKW7-2 wafer. For each testing die, the oxide thickness and step height were measured on five points in the step blocks with local pattern densities of 30, 70, and 50% (Fig. 5). Oxide thickness data were used to extract the necessary model parameters and simulate polishing performance of each pad using the physical die-level CMP model. We extracted model parameters by fitting to experimental data and by minimizing the fitting error from time split experiment data. The hypothesized pad property effects are seen clearly in the pad parameter and model simulation results, as discussed below.

Results and Discussion

We applied two different sets of experimental conditions to emphasize either the pad bulk dependence or the pad surface and asperity structure dependence. The reference pressure P_0 is 5 psi for both sets. In the first set of experiments, we polished wafers using pads with different stiffnesses (low, standard, and high), while we used the same conditioning disk. In the second set of experiments, we polished wafers using a standard pad, while we applied three different conditioning disks (sharp, standard, and blocky). The first set investigates pad stiffness effect, and the second set verifies pad conditioning effects.

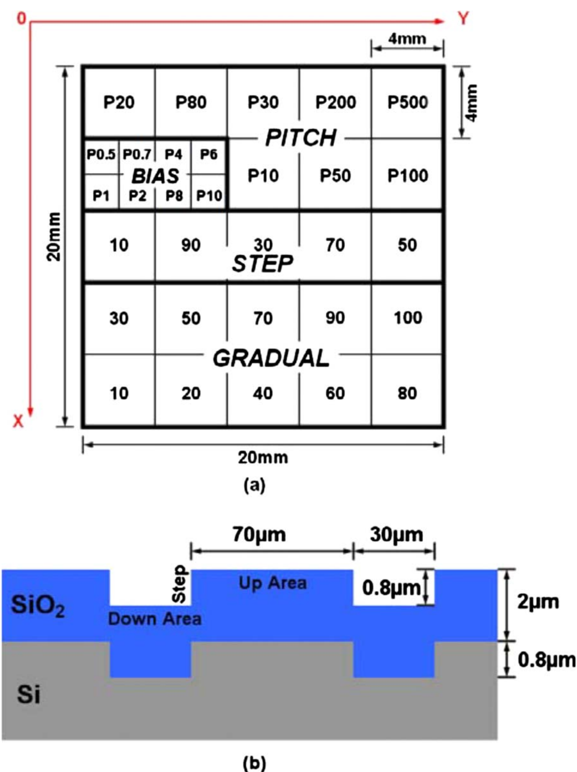

Figure 4. (Color online) Pattern type and pattern density within a die of SKW7-2 wafer: (a) Layout of a die on SKW7-2 wafer. A "P" preceding a number indicates a pitch structure with 50% density, with the number following in micrometers. All other numbers are localized densities, with the number indicating the density. Density structures have a fixed 100 μm pitch. (b) Topography of the 70% STEP array in a die.

CMP pad stiffness effect.— JSR pads with different stiffnesses (low, standard, and high) were tested by polishing experiments and model data fitting. Based on the physical model, fitting results were hypothesized to have different effective moduli but similar asperity heights and blanket removal rates. Figure 6 shows the extracted model parameters. As expected, effective modulus varies corresponding to the pad bulk stiffness. In addition, the characteristic asperity height and the blanket removal rate do not change substantially.

In the following discussion, we only focus on the middle die and do not consider in detail the across-wafer variation observed in the measured results. Our model here is die-level only and does not seek to account for CMP tool design or process nonuniformities in pressure, velocity, pad microstructure, conditioning profile, or other parameters across the wafer.[5,14,15] Nonuniformity in pad properties (such as effective modulus and asperity height distribution) resulting from wafer-level effects are of interest for future work.

A useful output from our model to reflect the main within-die uniformity effect of pad stiffness is the "nominal range," which is defined as the difference between the up-area oxide thickness of the 90% pattern-density area and that of the 10% pattern-density area.

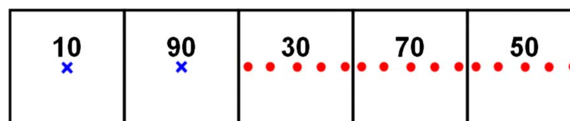

Figure 5. (Color online) Optical measurement positions in the STEP blocks in a die of SKW7-2 dielectric wafer. Dots indicate both thickness and step height measurements. Crosses indicate only step height measurement.

Downloaded 14 Jun 2012 to 18.51.3.76. Redistribution subject to ECS license or copyright; see http://www.ecsdl.org/terms_use.jsp

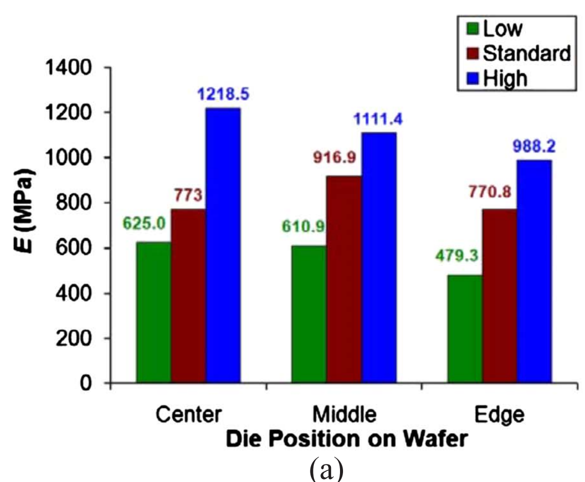

(a)

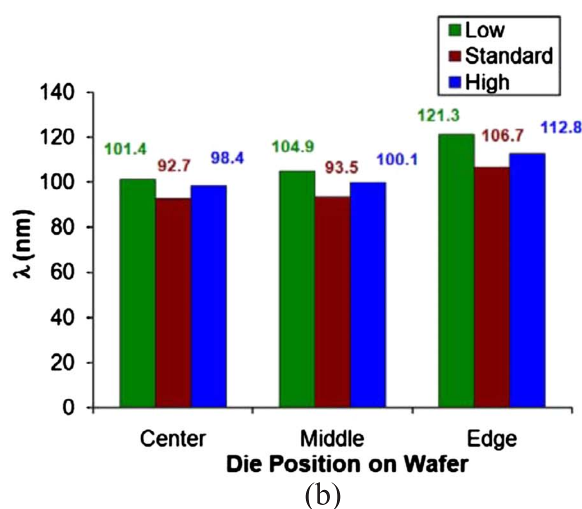

(b)

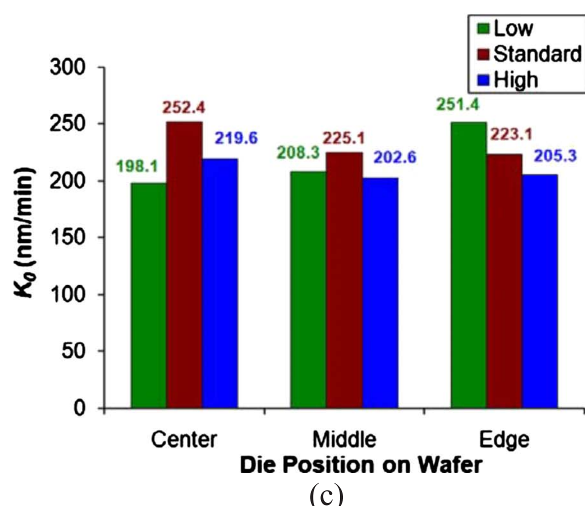

(c)

Figure 6. (Color online) Extracted model parameters for different pad stiffnesses: (a) Effective modulus, (b) characteristic asperity height, and (c) blanket removal rate.

Within-die nonuniformity results from faster removal rates in low pattern density regions on the die compared to high pattern density areas: The local pad force is applied to a smaller number of up features in the low pattern density region, generating much higher local pressure and resulting in a large "recessed" or "eroded" region

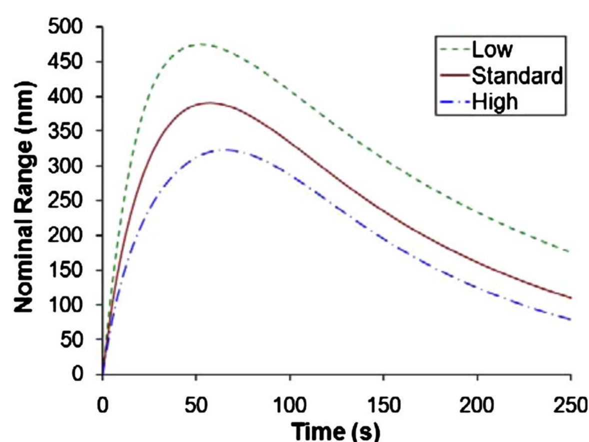

Figure 7. (Color online) Simulated middle die nominal range evolution for different pad stiffnesses.

on the die. Across lateral distances of several millimeters, this within-die nonuniformity can be substantial, with oxide thickness differences of several hundred nanometers. To combat this effect, pads with a higher stiffness are of interest, as they are subject to less long-range bending. Across the oxide step structures, hard pads deflect less into recessed low pattern density areas, reducing the regional polish rates compared to high pattern density regions, resulting in a smaller final nominal range, as shown in Fig. 7. In this figure, the creation of within-die nonuniformity in the first 50–70 s due to pattern density removal rate dependence is seen, with subsequent reduction as polishing progresses. At all times, the harder pads create a less nominal range between 90 and 10% region thicknesses.

We can also understand the pad stiffness effect vs asperity height effect by comparing step height evolution in the polishing process. Figure 8a shows the data fitting results of step height vs time on the center point of a middle die in the 50% pattern density array. We see that the high stiffness pad maintains a linear step height reduction region to a comparable remaining step height (at which point an exponential decay in time occurs) across all three pads, corresponding to our expectation that bulk pad stiffness is not the primary factor in individual feature step height removal or down-area polish. Comparing the step height evolution at the center (Fig. 8a), left edge (Fig. 8b), and right edge (Fig. 8c) points of the 50% pattern density array on the middle die, however, we see the pattern density dependence of polishing as expected. As indicated by the straight dashed lines, step height reaches to 200 nm with the remaining height moving slowly (at about 95 s) at the left edge point (next to 70% pattern density array) and moving quickly (at about 66 s) at the right edge point (next to 10% pattern density array). This is the result of the long-range pad bending, which results in different "effective" pattern densities at different points within the same local pattern density region, due to spatial "averaging" of the applied pad pressure across the die.

CMP pad conditioning effect.— JSR standard pads with different conditioning disk diamond types (blocky, standard, and sharp) were tested. Because we used the same type of pad, the extracted effective modulus is similar for each conditioning disk (Fig. 9a), as expected. Especially for the middle die, the modulus differences are very small (less than 2.5%). But the characteristic asperity height is consistently different (Fig. 9b); the characteristic asperity height varies according the to the diamond shape. The blanket removal rate does not change substantially (Fig. 9c).

In the conditioning test, the simulated nominal range (or within-die oxide thickness uniformity) based on the extracted model parameters is not significantly impacted by the characteristic asperity height, and thus, the range evolutions are similar for different conditioning disks (Fig. 10). However, there is a difference in step

Downloaded 14 Jun 2012 to 18.51.3.76. Redistribution subject to ECS license or copyright; see http://www.ecsdl.org/terms_use.jsp

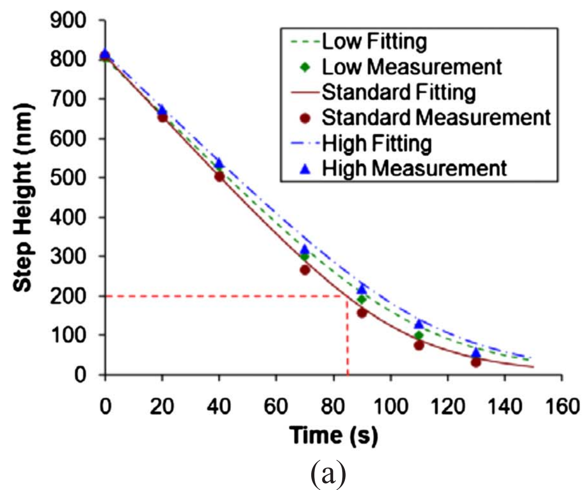

(a)

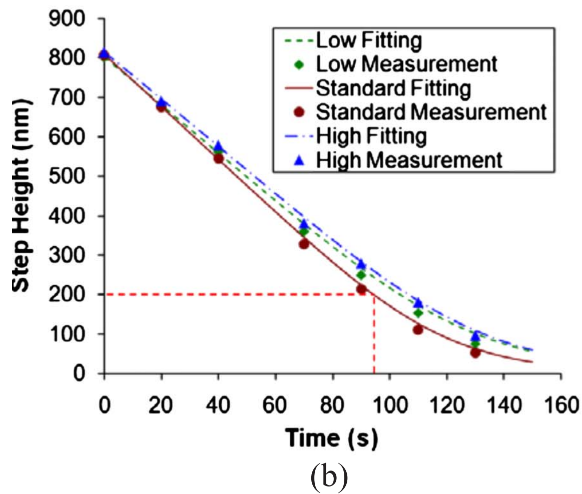

(b)

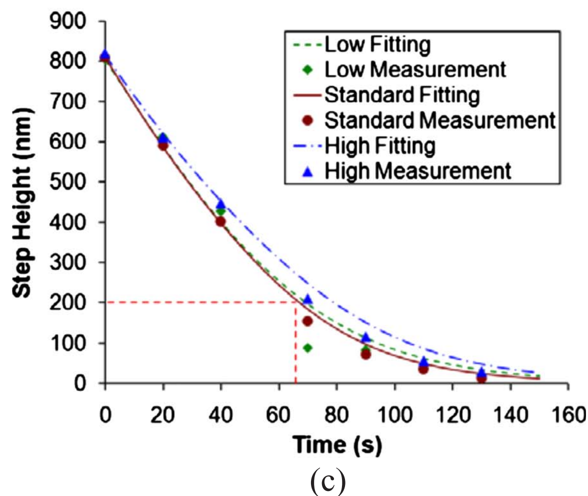

(c)

Figure 8. (Color online) Middle die 50% pattern density array step height evolution for different pad stiffnesses: (a) Center point, (b) left edge point (next to 70% pattern density array in Fig. 5), and (c) right edge point (next to 10% pattern density array in Fig. 5).

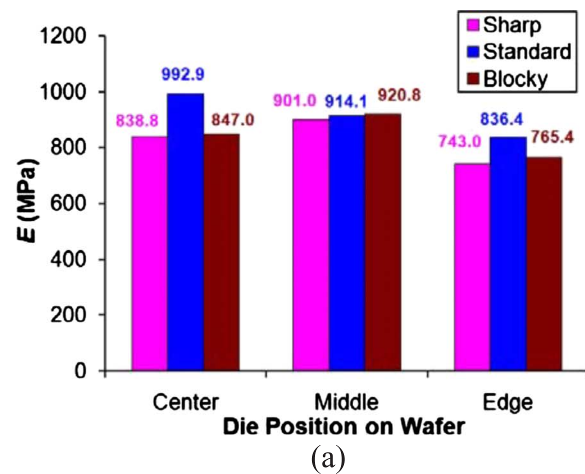

(a)

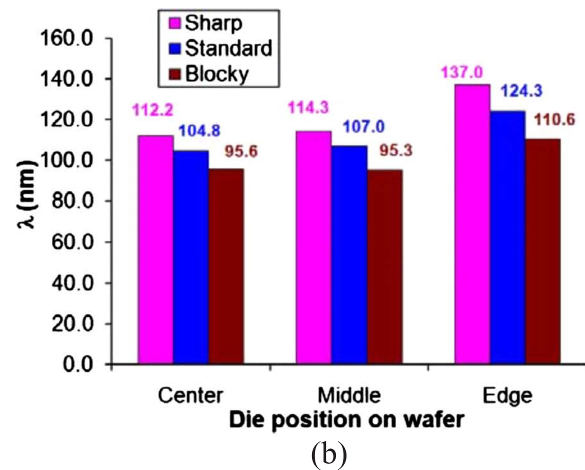

(b)

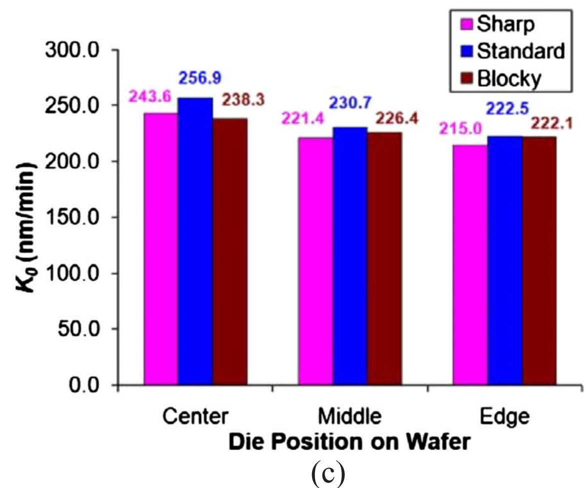

(c)

Figure 9. (Color online) Extracted model parameters for different conditioning disk diamond shapes: (a) Effective modulus, (b) characteristic asperity height, and (c) blanket removal rate.

height evolution. Figure 11 shows the data fitting result of step height vs time of the middle die 50% pattern density array. The pattern density dependence of the polish is also verified by comparing the step height evolution at the center (Fig. 11a), left edge (Fig. 11b), and right edge (Fig. 11c) points of the 50% pattern density array on the middle die. The sharp diamond disk data go to a nonlinear region slightly earlier (at a larger remaining step height) than the other disks. This transition in the linear step height reduction in time occurs when asperities start to polish both the up and down feature areas rather than just the up areas; we thus expect this transition to depend on the pad asperity height. A good way to understand the linear to nonlinear transition in step height is shown in Fig.

Downloaded 14 Jun 2012 to 18.51.3.76. Redistribution subject to ECS license or copyright; see http://www.ecsdl.org/terms_use.jsp

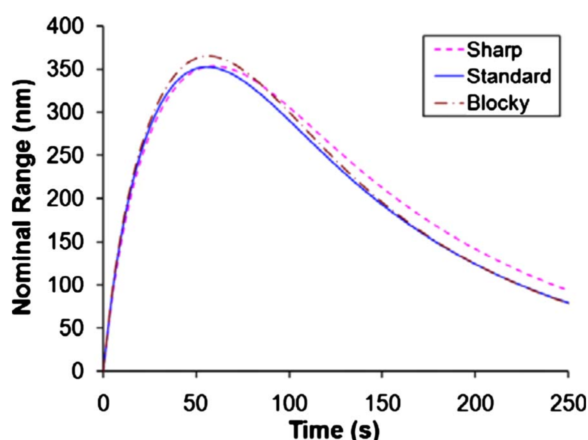

Figure 10. (Color online) Simulated middle die nominal range evolution for different conditioning disk diamond shapes.

12. In the beginning of the process, the down-area removal amount is zero. When the step height reduction goes to nonlinear, down area removal amount starts to increase above zero. In Fig. 12, the sharp disk curve goes to above zero at the largest remaining step height among the three disks, while the blocky disk curve goes to above zero at the lowest remaining step height. The characteristic asperity heights vary about 15% for the three conditioning disks, so we see a clear relationship verifying the physical model sensitivity to pad properties.

Simulation of CMP die-level uniformity and end point.— CMP is used to planarize the wafer surface to remove topography resulting from previous patterning and deposition processes. In practice, perfect planarization is difficult to achieve due to the pattern density differences on the die, where planarization of low density areas is faster than that of high density areas. In general, the CMP process must be stopped once a certain end-point strategy is fulfilled. In one approach, the polishing should stop when the original step height has been reduced to some value that is "small enough" to meet product requirements, which is called the step height target strategy. Another commonly used approach is thickness target strategy, in which the process should stop when the up-area thickness has been reduced to some value as product requirements.

To understand the die-level uniformity and impact on the process end point, a full chip simulation (middle die of Fig. 3) was run for pad conditioning effects using the JSR standard pad. The end point was defined as occurring when a step height target of 100 nm at the 50% pattern density area is reached, i.e., the polishing stops when the remaining step height is 100 nm at the center point of the 50% pattern density area. Table I lists the simulation results for the different diamond conditions. We can see the differences in final within-die and step height uniformity with these numbers. While the 50% pattern density area reaches the end point, the 10% pattern density area is overpolished and the 90% pattern density area still has a remaining step height substantially larger than the end-point target. From the end-point time, we see that the standard pad with a blocky conditioning disk planarizes faster, which corresponds to Fig. 11a. Table I also tells us that within-die oxide thickness uniformity is not substantially impacted by conditioning disks because both the nominal range (difference between the up-area oxide thickness of the 90% pattern-density area and that of the 10% pattern-density area) and the full chip range (difference between the maximum up-area thickness and the minimum up-area thickness across the entire chip) are similar for the three different disks. The full chip simulation of the middle die surface at the end point for the JSR standard pad with a standard conditioning disk is shown in Fig. 13. We see that the uniformity is affected significantly by pattern density. Although the STEP-90 array has a 90% pattern density, its final

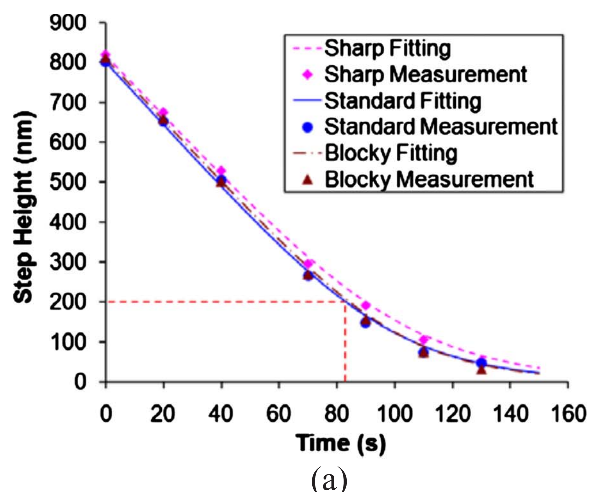

(a)

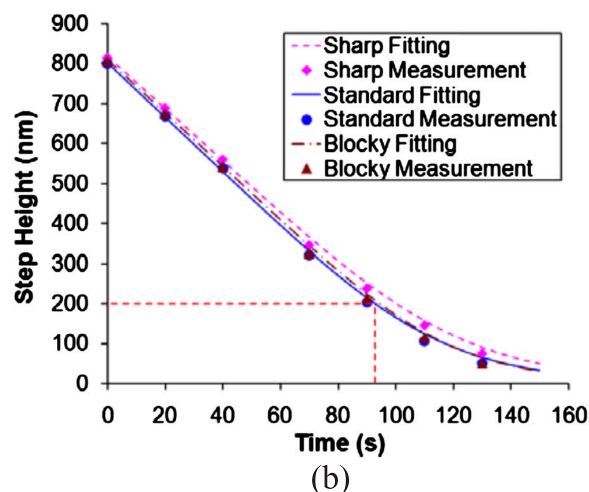

(b)

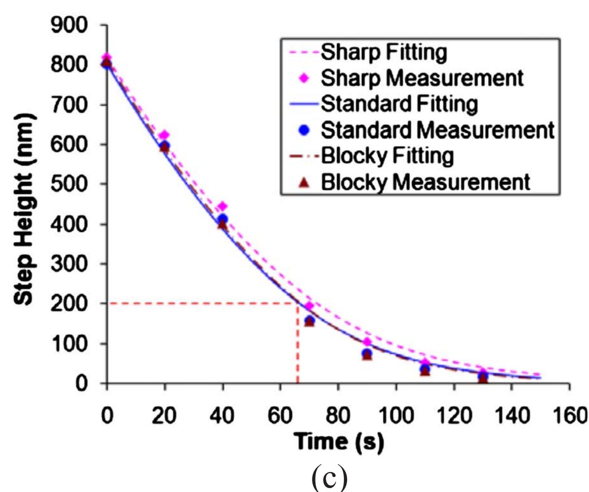

(c)

Figure 11. (Color online) Middle die 50% pattern density array step height evolution for different conditioning disks: (a) Center point, (b) left edge point (next to 70% pattern density array in Fig. 5), and (c) right edge point (next to 10% pattern density array in Fig. 5).

thickness and step height are not high. The reason is that its neighboring arrays have lower pattern densities (10 and 30%). The end point of thickness target strategy was defined as occurring when an up-area thickness of 1000 nm at the 50% pattern density area is reached; i.e., the process stops, and then the remaining up-area

Downloaded 14 Jun 2012 to 18.51.3.76. Redistribution subject to ECS license or copyright; see http://www.ecsdl.org/terms_use.jsp

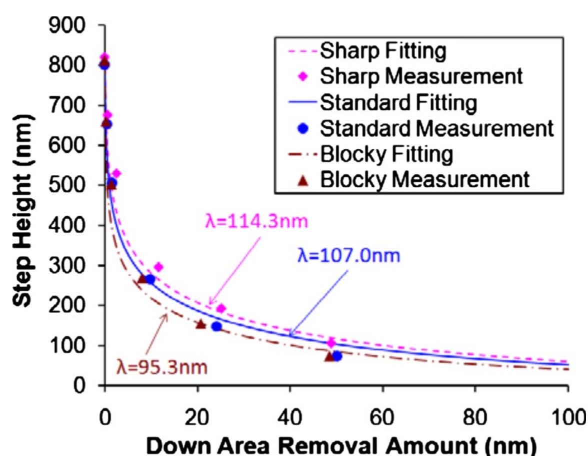

Figure 12. (Color online) Middle die 50% pattern density array center point step height vs down area removal amount for different conditioning disk diamond shapes. Take down area removal amount at 1 nm as the linear to nonlinear transition point. The remaining step heights of the blocky, standard, and sharp disks at the transition point are 436.0, 497.7, and 533.5 nm, respectively.

thickness is 1000 nm at the center point of the 50% pattern density area. Table II lists the simulation results of the thickness strategy for the different diamond conditioning disks. It is very easy to see the pattern-density-dependent within-die nonuniformity. The planarization efficiency of the blocky disk is higher than the other two because at the end point the remaining step height of the blocky disk is less than that of the others.

Conclusion

A physical die-level CMP model has been applied to the pad property and polish process analysis. The experimental results confirm the decomposition of the model between the pad bulk and pad asperity components. We are able to relate the pad stiffness and the conditioning disk effects to the model parameters and data fitting results. Quantitative relationships between pad properties and model parameters were established, which can be used to evaluate pad performance and to assist in pad design and optimization. Model prediction is the same as our expectation: A higher pad stiffness gives better within-die uniformity, and a conditioning disk with blocky diamonds keeps the linear polishing region longer. This physical CMP model correctly simulates pattern density dependence and within-die uniformity.

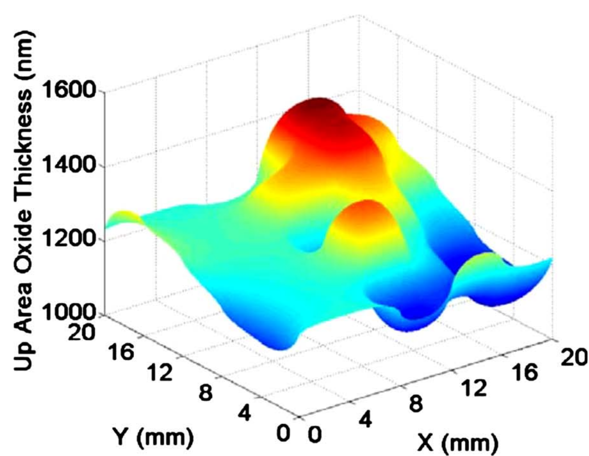

(a)

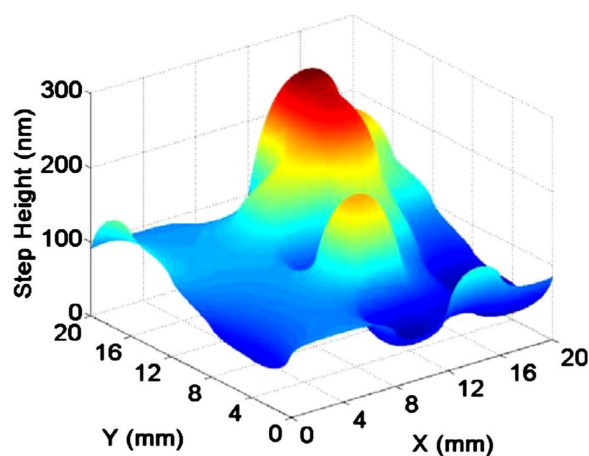

(b)

Figure 13. (Color online) Full chip simulation for the SKW7-2 test pattern at the time point when a 100 nm step height end point in the 50% pattern density region is reached. Simulation is for a JSR standard pad with a standard conditioning disk: (a) Up-area oxide thickness and (b) step height. The x-y coordinate corresponds to the layout shown in Fig. 4a.

Table I. Simulation results of step height target strategy for pad conditioning effects on JSR standard pad.

Conditioning disk diamond shape		Sharp	Standard	Blocky
Initial step height (nm)			800	
Initial up-area thickness (nm)			2000	
End-point time (s)		114	107	105
Remaining step height (nm)	Center point of 10% pattern density area	36.5	34.5	30.7
	Center point of 50% pattern density area		100 (end point)	
	Center point of 90% pattern density area	186.7	192.6	205.6
	Maximum	259.5	267.9	284.3
	Minimum	29.5	27.4	23.7
Nominal range (nm)		272.6	275.9	285.0
Full chip range (nm)		385.8	389.5	398.7
Up-area thickness (nm)	Center point of 10% pattern density area	1089.5	1097.6	1109.0
	Center point of 50% pattern density area	1237.2	1246.2	1261.1
	Center point of 90% pattern density area	1362.1	1373.4	1394.0
	Maximum	1447.3	1458.8	1479.5
	Minimum	1061.4	1069.4	1080.7

Downloaded 14 Jun 2012 to 18.51.3.76. Redistribution subject to ECS license or copyright; see http://www.ecsdl.org/terms_use.jsp

Table II. Simulation results of up-area thickness target strategy for pad conditioning effects on JSR standard pad.

Conditioning disk diamond shape		Sharp	Standard	Blocky
Initial step height (nm)			800	
Initial up-area thickness (nm)			2000	
End-point time (s)		170	163	165
Remaining step height (nm)	Center point of 10% pattern density area	8.1	6.5	4.4
	Center point of 50% pattern density area	18.0	15.0	10.9
	Center point of 90% pattern density area	33.9	29.2	23.2
	Maximum	65.3	59.7	53.0
	Minimum	6.4	5.0	3.3
Nominal range (nm)		176.6	172.0	168.4
Full chip range (nm)		295.4	291.7	289.7
Up-area thickness (nm)	Center point of 10% pattern density area	903.0	905.2	910.3
	Center point of 50% pattern density area		1000 (end point)	
	Center point of 90% pattern density area	1079.6	1077.2	1078.7
	Maximum	1171.1	1169.5	1172.4
	Minimum	875.7	877.8	882.7

Acknowledgments

The authors thank the GRC/SEMATECH Joint Engineering Research Center for Environmentally Benign Semiconductor Manufacturing for providing support for this work.

Massachusetts Institute of Technology assisted in meeting the publication costs of this article.

References

1. J. M. Steigerwald, S. P. Murarka, and R. J. Gutmann, *Chemical Mechanical Planarization of Microelectronic Materials*, p. 4, John Wiley & Sons, New York (1997).
2. D. Evans, *MRS Bull.*, **27**, 779 (2002).
3. R. K. Singh and R. Bajaj, *MRS Bull.*, **27**, 743 (2002).
4. G. Nanz and L. E. Camilletti, *IEEE Trans. Semicond. Manuf.*, **8**, 382 (1995).
5. X. Xie, Ph.D. Thesis, Massachusetts Institute of Technology, Cambridge (2007).
6. O. G. Chekina and L. M. Keer, *J. Electrochem. Soc.*, **145**, 2100 (1998).
7. T. Yoshida, in *Chemical Mechanical Polishing in IC Device Manufacturing III*, Y. A. Arimoto, R. L. Opila, C. Reidsema Simpson, K. B. Sundaram, I. Ali, and Y. Homma, Editors, PV 99-37, p. 593, The Electrochemical Society Proceedings Series, Pennington, NJ (1999).
8. L. Borucki, R. Zhuang, T. Sun, Y. Zhuang, A. Philipossian, and D. Slutz, in *International Conference on Planarization Technology*, Northern California Chapter of the American Vacuum Society CMP Users Group (2006).
9. F. Preston, *J. Soc. Glass Technol.*, **11**, 214 (1927).
10. http://www.jsrmicro.com/pro_CMP_pad.html, last accessed Feb 2010.
11. http://www.jsr.co.jp/jsr_e/pd/images/pad.pdf, last accessed Feb 2010.
12. L. Charns, M. Sugiyama, and A. Philipossian, *Thin Solid Films*, **485**, 188 (2005).
13. http://www.testwafer.com/PDF/skw7-2.pdf, last accessed Feb 2010.
14. J. Luo and D. A. Dornfeld, *Integrated Modeling of Chemical Mechanical Planarization for Sub-Micron IC Fabrication*, p. 264, Springer, Berlin (2004).
15. S. Lo, Y. Lin, and J. Huang, *Int. J. Adv. Manuf. Technol.*, **34**, 547 (2007).

Downloaded 14 Jun 2012 to 18.51.3.76. Redistribution subject to ECS license or copyright; see http://www.ecsdl.org/terms_use.jsp